

Rotating halo traced by the K giant stars from LAMOST and Gaia

HAO TIAN,¹ CHAO LIU,¹ AND YAN XU¹XIANGXIANG XUE¹¹*Key Laboratory of Optical Astronomy,
National Astronomical Observatories, Chinese Academy of Sciences,
Datun Road 20A, Beijing 100012, PR China;*

(Received March 31, 2022; Revised March 31, 2022; Accepted —)

Submitted to —

ABSTRACT

With the help of Gaia DR2, we are able to obtain the full 6-D phase space information for stars from LAMOST DR5. With high precision of position, velocity, and metallicity, the rotation of the local stellar halo is presented using the K giant stars with $[\text{Fe}/\text{H}] < -1$ dex. By fitting the rotational velocity distribution with three Gaussian components, stellar halo, disk, and a counter-rotating hot population, we find that the halo progradely rotates with $V_T = +30 \pm 4 \text{ km s}^{-1}$ providing the local standard of rest velocity of $V_{LSR} = 232 \text{ km s}^{-1}$. Meanwhile, we obtain the dispersion of rotational velocity is $\sigma_T = 77 \pm 4 \text{ km s}^{-1}$ and the local anisotropy of the halo is ~ 0.7 . Although the rotational velocity strongly depends on the choice of V_{LSR} , the trend of prograde rotation is substantial even when V_{LSR} is set at as low as 220 km s^{-1} . Moreover, we derive the rotation for subsamples with different metallicities and find that the rotational velocity is essentially not correlated with $[\text{Fe}/\text{H}]$. This may hint a secular evolution origin of the prograde rotation. It shows that the metallicity of the progradely rotating halo is peaked within $-1.9 < [\text{Fe}/\text{H}] < -1.6$ without considering the selection effect. We also find a small fraction of counter-rotating stars with larger dispersion and lower metallicity. Finally, the disk component rotates with $V_T = +185 \pm 5 \text{ km s}^{-1}$ and $\sigma_T = 44 \pm 3 \text{ km s}^{-1}$, which is quite consistent with the metal-weak thick disk population.

Keywords: galaxies: individual (Milky Way) — Galaxy: kinematics and dynamics — Galaxy: halo — Stars: individual (K-giants)

1. INTRODUCTION

It has been widely accepted that the Milky Way, at least the halo, was formed through hierarchically merging smaller stellar systems, such as globular clusters and dwarf galaxies (Belokurov et al. 2006). With a long time evolving, the stellar members of those merged systems will be continuously stripped and then form stellar streams (Johnston et al. 1999). Such phenomena have been widely searched with photometric sky surveys, e.g. SDSS (York et al. 2000) and Pan-STARRS (Bernard

et al. 2016). Since the first stellar stream, Sagittarius stream, discovered by Ibata et al. (1994), many streams have been discovered with matched filter method (Rockosi et al. 2002; Grillmair & Carlin 2016; Grillmair & Dionatos 2006a,b,c; Grillmair 2009) and other methods (Mateu et al. 2018). But the streams are not the final fate of those merged clusters or dwarf galaxies, a longer evolving time will make the streams more and more relaxed and finally become part of the smoothing halo, i.e. it is not visible in the geometric space (Helmi et al. 1999), even blurred in the phase space (Helmi & de Zeeuw 2000; Sanderson et al. 2015).

Assuming those merged stellar systems fell in with random orbits (Sanderson et al. 2015), the contribution of z -axis angular momentum L_z overall should be

Corresponding author: Hao Tian (LAMOST FELLOW), Chao Liu
tianhao@nao.cas.cn, liuchao@nao.cas.cn

around 0. The net angular momentum is directly related to the merging history. Another possibility is that the merged halo was driven to slowly rotate by the non-axisymmetric structure in the disk (e.g. bar) in a long time scale (Athanasoula et al. 2013).

The studies on signal of rotation have been done since 1980s (Frenk & White 1980). Morrison et al. (1990) studied the kinematics of the halo and disk using the G and K giant stars within 4 kpc from the Sun, and claimed a prograde rotation of $V_T = 25 \pm 15 \text{ km s}^{-1}$. They also showed that the metallicity of the thick disk stars can be as low as -1.6.

Smith et al. (2009) studied the kinematics of the halo and found that the stellar halo exhibits no rotation with rotational velocity V_ϕ dispersion $82 \pm 2 \text{ km s}^{-1}$. Deason et al. (2017) used the 3D velocity calculated from the proper motion of different tracers from *Gaia* Data Release (hereafter *GDR*) 1 and SDSS dataset to study the halo rotation. A prograde rotation was found with $V_T = 14 \pm 2 \pm 10 \text{ km s}^{-1}$. What is more, the metal richer stars are showing a stronger prograde rotation which is explained as a small fraction of halo stars formed in situ. Kafle et al. (2017) also found a similar trend with only radial velocity. What is different is that the metal poorer K giant stars show a retrograde rotation.

GDR2 (Gaia Collaboration et al. 2018a,b,c,d,e,f) contains ~ 1.3 billion stars high accuracy proper motions and parallaxes, which have brought a series of amazing results about the halo, such as the velocity determination of globular clusters and rotation curve of the Large Magellanic Cloud (Gaia Collaboration et al. 2018e). Besides, Gaia Collaboration et al. (2018e) also derived a lower limit total mass for the Milky Way.

Guoshoujing Telescope (the Large Sky Area Multi-Object Fiber Spectroscopic Telescope, hereafter LAMOST) is a 4-meter, quasi-meridian, reflecting Schmidt telescope which makes it an efficient spectroscopic telescope (Cui et al. 2012; Deng et al. 2012; Zhao et al. 2012). Liu et al. (2017) and Xu et al. (2018) used metal poor K giants from LAMOST to trace the density profile of the halo and found an inner oblate, outer nearly spherical profile. Recently, LAMOST has released its 5th data (DR5). As low resolution of $R = 1800$, the uncertainties of T_{eff} and $[\text{Fe}/\text{H}]$ are typical $\sim 100 \text{ K}$ and $\sim 0.1 \text{ dex}$, respectively, for the stellar spectra with signal to noise ratio larger than 30.

The paper studies the rotation of the local stellar halo using the combination of the GDR2 and LAMOST DR5 K-giant stars and is constructed as follow. In Section 2, the sample stars are selected. The model of the distribution of rotational velocity is developed in Section 3. The

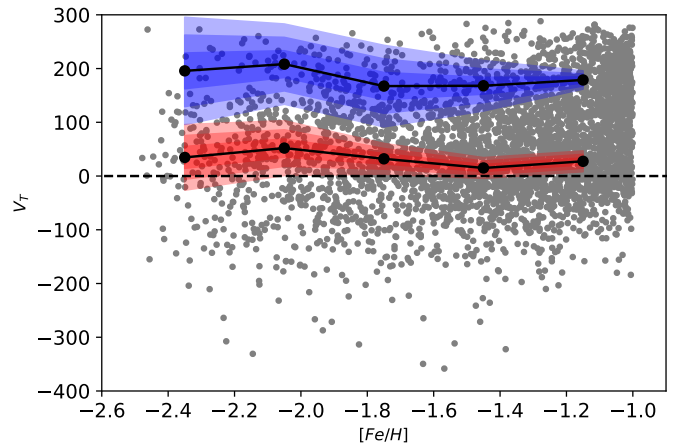


Figure 1. The rotational velocity distribution of the K giant stars is shown as the gray dots. The black solid lines in the blue and red shaded regions indicate the rotational velocities of the disk and halo components, respectively. The shadow colors from heavy to light represent the uncertainties from 1σ to 3σ .

results are discussed in Section 4. The conclusions are listed in Section 5.

2. DATA SAMPLE

In this work, we use K giant stars selected from LAMOST DR5 based on the criteria suggested by Liu et al. (2014) to study the kinematics of the nearby halo. After cross-matching with GDR2, we obtained the parallax, proper motions, radial velocities and metallicities for the tracer stars. A robust metallicity cut with $[\text{Fe}/\text{H}] < -1$ is used to remove the majority of disk stars, which leaves 6660 K giant stars. With the distances from Bailer-Jones et al. (2018), the samples within 4 kpc and relative distance error $D_{\text{error}}/D < 0.2$ are further selected so that the distance estimates are reliable, and 3827 stars are left in the sample. Comparing the radial velocities between GDR2 and LAMOST, we find an offset $RV_{\text{Gaia}} - RV_{\text{LAMOST}}$ of 5.38 km s^{-1} , which was also mentioned by Tian et al. (2015) and Schönrich & Aumer (2017). To avoid this systematics, we adopt the radial velocity provided by GDR2. In the final dataset, the median errors of proper motion in RA and DEC are 0.065 and $0.054 \text{ mas yr}^{-1}$, respectively. The median error of radial velocity is 1.0 km s^{-1} . Figure 1 shows the final samples in rotational velocity (V_T) versus $[\text{Fe}/\text{H}]$ plane.

We use *galpy* (Bovy 2015) to calculate the 3D locations in heliocentric cartesian coordinates, X , Y , Z , and velocity components in galactocentric cylindrical coordinates, radial component V_R , rotational (azimuthal) component V_T , and vertical component V_Z . By default, we adopt the velocity of the local standard of rest (LSR)

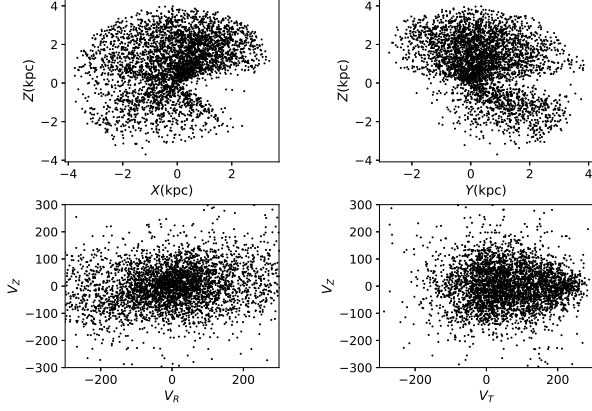


Figure 2. Distributions of the sample in geometric space (top panels) and velocity space (bottom panels).

with respect to the Galactic center as $V_{LSR} = 232 \text{ km s}^{-1}$ (McMillan 2017) and the solar motion with respect to the LSR as $(U_{\odot}, V_{\odot}, W_{\odot}) = (11.1, 12.24, 7.25) \text{ km s}^{-1}$ (Schönrich et al. 2010).

Figure 2 shows the distributions of the selected K giant stars in geometric (top panels) and velocity (bottom panels) spaces. The samples do not show disk-like features, implying that most of the disk stars are removed by the cut in $[\text{Fe}/\text{H}]$. The top panels show that the stars are rarely sampled at $X > 0$, $Y > 0$, and $Z \sim 0$, which is caused by the observational limit of LAMOST survey. This would not affect the detection of the rotation of the halo. The bottom-left panel shows that the distribution in V_R versus V_Z space is quite smooth. And the bottom-right panel displays an excess with V_T at around 200 km s^{-1} , which may be the slight contamination of the thick disk.

3. MODEL OF THE DISTRIBUTION OF V_T

In Figure 3, it is seen that the distribution of V_T for the samples (black dots with error bars) shows two peaks and a long tail beyond $V_T < -200 \text{ km s}^{-1}$. This hints that it may contain three components. The most dominated component shows up a peak located just at the right side of $V_T = 0$. The second component contributes a metal-rich peak at around 200 km s^{-1} . And the third one, maybe a broad one, contributes to the long tail at $V_T < -200 \text{ km s}^{-1}$, especially at metal poor end. By convenience, we assume all the three components are Gaussians and their distribution of V_T can be defined as

$$p_i(V_T | f_i, V_{T,i}, \sigma_i) = \frac{f_i}{\sqrt{2\pi}\sigma_i} \exp\left(-\frac{(V_T - V_{T,i})^2}{2\sigma_i^2}\right), \quad (1)$$

where $i = 1, 2, 3$ represent for the three components, f_i , $V_{T,i}$, and σ_i stand for the fraction, mean velocity, and velocity dispersion for the i th component, respectively.

According to Bayes' theorem, the posterior probability distribution of the unknown parameters can be written as

$$p(\theta_1, \theta_2, \theta_3 | V_T) \propto \prod_{k=1}^n \sum_{i=1}^3 p_i(V_T^{(k)} | \theta_i) p(\theta_1, \theta_2, \theta_3), \quad (2)$$

where $\theta_i = (f_i, V_{T,i}, \sigma_i)$ is the parameter vector for the i th component. k represents for the k th star in the samples with totally n stars. We adopt simplistic and loose priors such that $0 < f_i < 1$, $-100 < V_{T,1}, V_{T,3} < 100 \text{ km s}^{-1}$, $100 < V_{T,2} < 300 \text{ km s}^{-1}$, and $\sigma_i < 200 \text{ km s}^{-1}$. We further require $f_1 + f_2 + f_3 = 1$ so that f_3 is not a free parameter but derived from f_1 and f_2 . Therefore, we totally have 8 free parameters in the model, i.e. $f_1, f_2, V_{T,1}, V_{T,2}, V_{T,3}, \sigma_{T,1}, \sigma_{T,2}$, and $\sigma_{T,3}$.

Then we apply *emcee* (Foreman-Mackey et al. 2013) to run a Markov chain Monte Carlo (MCMC) simulation for Eq. (2). Figure 4 shows the results of the MCMC. We adopt the median values and standard deviations of the MCMC samples as the best-fit parameters and their uncertainties and show the best-fit models in the top-left panel of Figure 3. The first row of Table 1 lists the best-fit parameters and their uncertainties of the three Gaussians.

4. RESULT

4.1. Identification of the three components

The 1st component with $V_{T,1} = 30 \pm 4 \text{ km s}^{-1}$ and $\sigma_{T,1} = 77 \pm 4 \text{ km s}^{-1}$ is likely the stellar halo population, since the dispersion is quite similar to Smith et al. (2009) and Bird et al. (2018) at galactocentric distance of 10 kpc. The 2nd component shows quite faster rotation with $V_{T,2} = 185 \pm 5 \text{ km s}^{-1}$ and smaller dispersion $\sigma_{T,2} = 44 \pm 3 \text{ km s}^{-1}$. It is noted that Morrison et al. (1990) claimed that the *metal-weak thick disk* has rotational velocity of $V_T = 170 \pm 15 \text{ km s}^{-1}$. Therefore, this component is quite likely the metal-weak thick disk. The 3rd component shows retrograde rotation with $V_{T,3} = -94 \pm 44 \text{ km s}^{-1}$ and larger dispersion of $128 \pm 17 \text{ km s}^{-1}$. As we see in Section 4.3, this population has lower metallicity than the other two. It is either the so-called outer halo (Carollo et al. 2007) or an accreted debris in the solar neighborhood. In this work we focus on the stellar halo, i.e. the 1st component.

4.2. The rotation of the local stellar halo

The stellar halo with the heliocentric distance of 4 kpc (the 1st component) shows a significant prograde rotation of $30 \pm 4 \text{ km s}^{-1}$. Comparing to other works, such rotation is different with the value from Deason et al. (2017) and the value for K giant samples from Kafle et

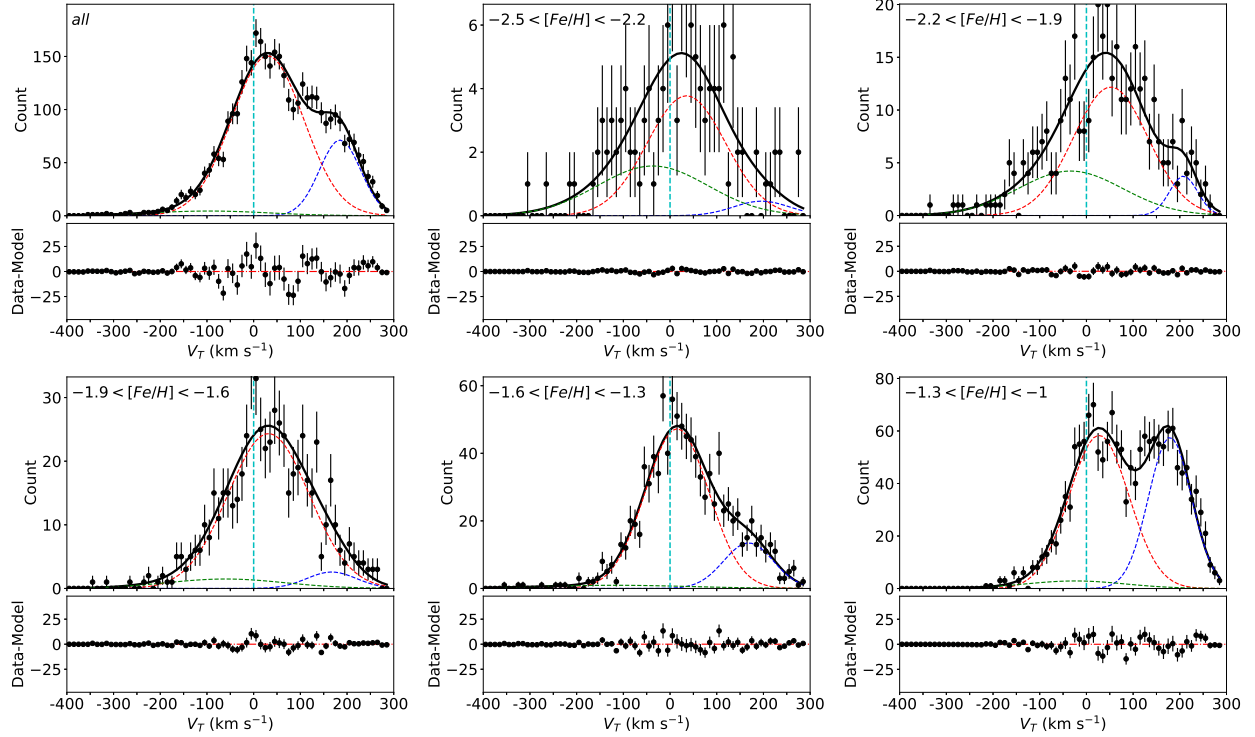


Figure 3. The top-left panel shows the distribution of V_T for all the sample stars (black dots). The error bars are derived from Poisson distribution. The bin size is set at 10 km s^{-1} . The red, blue, and green dashed lines indicate the best-fit Gaussian components $i = 1, 2$, and 3 respectively. The thick black solid line indicates the total distribution of the three-Gaussian model. The lower plot in the panel shows the residual distribution between the data and the model. No significant substructure is found in the residuals. The other panels are similar to the top-left one but for different $[\text{Fe}/\text{H}]$ bins. From top-middle to the bottom-right, the panels show the distribution of V_T and the corresponding best-fit models with metallicity bins of $-2.5 < [\text{Fe}/\text{H}] < -2.2$, $-2.2 < [\text{Fe}/\text{H}] < -1.9$, $-1.9 < [\text{Fe}/\text{H}] < -1.6$, $-1.6 < [\text{Fe}/\text{H}] < -1.3$, and $-1.3 < [\text{Fe}/\text{H}] < -1.0$, respectively.

al. (2017). Morrison et al. (1990) also studied the halo and disk with K giant stars and found that the stellar halo with $[\text{Fe}/\text{H}] < -1.6$ progradely rotates with $25 \pm 15 \text{ km s}^{-1}$, while the dispersion they detected is at $98 \pm 13 \text{ km s}^{-1}$, slightly larger than this work.

We also fit the other two velocity components and find that $\sigma_R = 173 \pm 22 \text{ km s}^{-1}$ and $\sigma_Z = 104 \pm 3 \text{ km s}^{-1}$ for the halo component. Consequently, we can directly obtain the local anisotropy parameter $\beta = 1 - \frac{\sigma_Z^2 + \sigma_{V_T}^2}{2\sigma_R^2}$ as around ~ 0.7 , which is in well agreement with the latest results by Bird et al. (2018).

4.3. V_T versus metallicity

Deason et al. (2017) used accurate proper motion to study the rotational velocity of halo stars and argued that the prograde rotation of the metal richer K giants is faster than that of the metal poorer sample. Kafle et al. (2017) also obtained a similar trend, but the difference is not significant. In light of those works, we detect the rotational velocity for the sub-samples with different metallicities.

We separate the samples into five sub-groups with $-2.5 < [\text{Fe}/\text{H}] < -2.2$, $-2.2 < [\text{Fe}/\text{H}] < -1.9$, $-1.9 < [\text{Fe}/\text{H}] < -1.6$, $-1.6 < [\text{Fe}/\text{H}] < -1.3$, and $-1.3 < [\text{Fe}/\text{H}] < -1.0$. For each sub-sample, similar MCMC simulation is applied and the best-fit 3-Gaussian model parameters are listed in Table 1. The comparison between the observed distributions of V_T and the models for different metallicities are displayed in Figure 3.

The black line with red shadows in Figure 1 indicates $V_{T,1}$ as a function of $[\text{Fe}/\text{H}]$ for the halo population (the 1st component). Rather than an increasing rotational velocity with the metallicity argued by previous works, this result prefers to an essentially flat relation between $V_{T,2}$ and $[\text{Fe}/\text{H}]$. In other word, we do not find the rotation of the local stellar halo is substantially correlated with metallicity.

It is worthy to note that the K giant samples used by Deason et al. (2017) are within 50 kpc and $|z| > 4 \text{ kpc}$ and the samples used by Kafle et al. (2017) are within 17 kpc and $|z| > 4 \text{ kpc}$. Neither of them is spacially overlapping with our sample.

The fraction f_1 of the halo population seems also independent of $[\text{Fe}/\text{H}]$, as seen in the corresponding col-

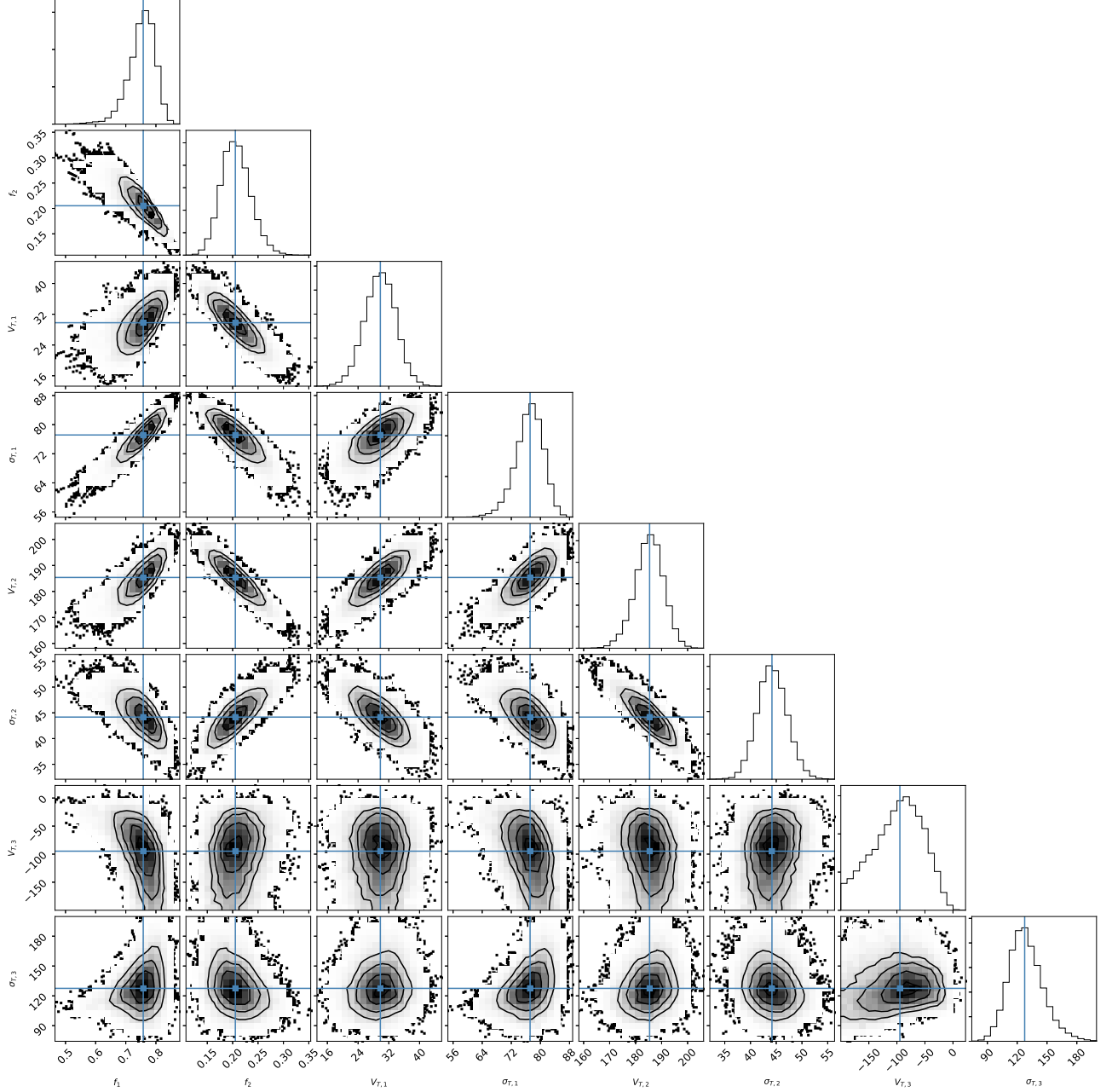


Figure 4. The results the MCMC simulation. The correlations of any two parameters are shown in the *corner* plot. The cyan lines are the median values of each individual parameters.

umn of Table 1. However, we find that f_1 is peaked at $-1.9 < [\text{Fe}/\text{H}] < -1.6$, implying that the mean metallicity of the 1st component is in this range. This again confirms that this component should be the stellar halo. Note that the selection effect in $[\text{Fe}/\text{H}]$ is not taken into account.

The black line in the blue shadow in Figure 1 shows rotational velocities at different metallicity bins for the disk component (the 2nd component). It is seen that the uncertainties of $V_{T,2}$ become smaller at metal richer

side. This is because the fraction of the disk becomes larger when $[\text{Fe}/\text{H}]$ increases, as seen in the column f_2 of Table 1. Thus more stars are involved in this component. This supports that the component has higher metallicity than the halo population.

Finally, f_3 column in Table 1 shows that the counter-rotational component occupies about one third at $-2.5 < [\text{Fe}/\text{H}] < -2.2$ and only contributes 4.6% at $-1.3 < [\text{Fe}/\text{H}] < -1.0$. This means that it is contributed by the most metal-poor stars. The averaged metallic-

Table 1. Best fit parameters of 3-Gaussian Models derived from MCMC.

	f_1	f_2	f_3	$V_{T,1}$ km s ⁻¹	$\sigma_{T,1}$ km s ⁻¹	$V_{T,2}$ km s ⁻¹	$\sigma_{T,2}$ km s ⁻¹	$V_{T,3}$ km s ⁻¹	$\sigma_{T,3}$ km s ⁻¹
all	0.758±0.045	0.205±0.029	0.037	30±4	77±4	185±5	44±3	-95±44	128±17
-2.5<[Fe/H]<-2.2	0.599±0.231	0.052±0.051	0.349	35±20	84±19	196±33	60±23	-37±48	118±24
-2.2<[Fe/H]<-1.9	0.625±0.173	0.072±0.054	0.303	52±17	80±12	208±25	30±16	-34±40	112±17
-1.9<[Fe/H]<-1.6	0.867±0.104	0.056±0.058	0.077	32±10	87±7	167±25	53±17	-60±51	127±26
-1.6<[Fe/H]<-1.3	0.788±0.056	0.175±0.050	0.037	15±6	68±5	168±16	53±7	-118±50	162±22
-1.3<[Fe/H]<-1.0	0.558±0.066	0.396±0.042	0.046	27±6	64±7	179±6	46±3	-24±35	107±17

ity of the component may be even lower than the halo population. This is consistent with Carollo et al. (2007) that the outer halo has metallicity of ~ -2.2 dex and in counter-rotation.

4.4. Possible mechanism of the prograde rotation of the stellar halo

The flat relationship between $V_{T,1}$ and [Fe/H] implies that the prograde rotation may not be originated from the sustained angular momenta of the minor mergers, but in favor of an effect of secular evolution. Indeed, Athanassoula et al. (2013) suggested that the rotating bar in the central region of the Galactic disk may transfer angular momenta to the halo. It is also noted that Xu et al. (2018) found the halo is oblate with axis-ratio lower than 0.5 at around 10 kpc, which may be related to the rotation of the halo.

4.5. Impact from parameter choices

As the LSR velocity brings a directly change in the rotational velocity during the conversion from proper motions, radial velocities and distances, we test the effect of different choices of V_{LSR} . We select three V_{LSR} values from literatures, 240 km s⁻¹ (Reid et al. 2014), 232 km s⁻¹ (Schönrich et al. 2010) and 220 km s⁻¹ (Dehnen 2000) for the test. We obtain that $V_T = 37 \pm 4$, 30 ± 4 , and 18 ± 4 km s⁻¹ for $V_{LSR} = 240$, 232, and 220 km s⁻¹, respectively. It is clear that a larger V_{LSR} leads to a higher halo rotation speed. However, even with the minimum value of $V_{LSR}=220$ km s⁻¹, the stellar halo is still in substantially prograde rotation. Moreover, we also find that the rotational velocity is essentially independent of the metallicity with different V_{LSR} .

5. CONCLUSION

We have studied the rotation of the halo with local K giant star samples within 4 kpc. Using the proper motions and radial velocities from *Gaia* and metallicities from LAMOST, we draw the following conclusions.

Firstly, the rotational velocity of the local stellar halo is strongly correlated to the LSR speed, V_{LSR} , and also

the azimuthal velocity of the Sun, V_\odot . With $V_{LSR} = 232$ km s⁻¹ and $V_\odot=12.24$ km s⁻¹, the halo is progradely rotating with $V_T = 30 \pm 4$ km s⁻¹. The dispersion of V_T of the halo K giant stars is $\sigma_{V_T} = 77 \pm 4$ km s⁻¹. We roughly derive the anisotropy of the halo population and obtain ~ 0.7 .

Secondly, we find that the rotational velocity of the stellar halo is independent of the metallicity in the local volume, which is different with the results in the outer volume claimed by Deason et al. (2017) and Kafle et al. (2017). The flat relationship between V_T and [Fe/H] hints that the rotation may be due to secular rotation, rather than due to the net angular momenta from the minor mergers.

Finally, we also identified a metal-poor and counter-rotating hot component with rotational velocity of -95 ± 44 km s⁻¹, which is likely the outer halo. And a disk-like component rotating with $V_T=185 \pm 5$ km s⁻¹ is also identified, which is likely the metal-weak thick disk.

This work is supported by the National Key Basic Research Program of China 2014CB845700. CL acknowledges the NSFC under grants 11373032 and 11333003. Guoshoujing Telescope (the Large Sky Area Multi-Object Fiber Spectroscopic Telescope LAMOST) is a National Major Scientific Project built by the Chinese Academy of Sciences. Funding for the project has been provided by the National Development and Reform Commission. LAMOST is operated and managed by the National Astronomical Observatories, Chinese Academy of Sciences. The LAMOST FELLOWSHIP is supported by Special Funding for Advanced Users, budgeted and administrated by Center for Astronomical Mega-Science, Chinese Academy of Sciences (CAMS). This work has made use of data from the European Space Agency (ESA) mission *Gaia* (<https://www.cosmos.esa.int/gaia>), processed by the *Gaia* Data Processing and Analysis Consortium (DPAC, <https://www.cosmos.esa.int/web/gaia/dpac/consortium>). Funding for the DPAC has been provided by national institutions, in particular the institutions

participating in the *Gaia* Multilateral Agreement. X.-X

Xue thanks the "Recruitment Program of Global Youth Experts" of China and NSFC 11390371.

REFERENCES

- Athanassoula, E., Machado, R. E. G., & Rodionov, S. A. 2013, *MNRAS*, 429, 1949
- Bailer-Jones, C. A. L., Rybizki, J., Fouesneau, M., Mantelet, G., & Andrae, R. 2018, arXiv:1804.10121
- Belokurov, V., Zucker, D. B., Evans, N. W., et al. 2006, *ApJL*, 642, L137
- Bernard, E. J., Ferguson, A. M. N., Schlafly, E. F., et al. 2016, *MNRAS*, 463, 1759
- Bird, S. A., Xue, X.-X., Liu, C., et al. 2018, arXiv:1805.04503
- Carollo, D., Beers, T. C., Lee, Y. S., et al. 2007, *Nature*, 450, 1020
- Bovy, J. 2015, *ApJS*, 216, 29
- Cui, X.-Q., Zhao, Y.-H., Chu, Y.-Q., et al. 2012, *Research in Astronomy and Astrophysics*, 12, 1197
- Deason, A. J., Belokurov, V., Koposov, S. E., et al. 2017, *MNRAS*, 470, 1259
- Dehnen, W. 2000, *AJ*, 119, 800
- Deng, L.-C., Newberg, H. J., Liu, C., et al. 2012, *Research in Astronomy and Astrophysics*, 12, 735
- Foreman-Mackey, D., Hogg, D. W., Lang, D., & Goodman, J. 2013, *PASP*, 125, 306
- Frenk, C. S., & White, S. D. M. 1980, *MNRAS*, 193, 295
- Gaia Collaboration, Eyer, L., Rimoldini, L., et al. 2018, arXiv:1804.09382
- Gaia Collaboration, Helmi, A., van Leeuwen, F., et al. 2018, arXiv:1804.09381
- Gaia Collaboration, Katz, D., Antoja, T., et al. 2018, arXiv:1804.09380
- Gaia Collaboration, Spoto, F., Tanga, P., et al. 2018, arXiv:1804.09379
- Gaia Collaboration, Babusiaux, C., van Leeuwen, F., et al. 2018, arXiv:1804.09378
- Gaia Collaboration, Brown, A. G. A., Vallenari, A., et al. 2018, arXiv:1804.09365
- Grillmair, C. J. 2009, *ApJ*, 693, 1118
- Grillmair, C. J., & Carlin, J. L. 2016, *Tidal Streams in the Local Group and Beyond*, 420, 87
- Grillmair, C. J., & Dionatos, O. 2006, *Bulletin of the American Astronomical Society*, 38, 48.03
- Grillmair, C. J., & Dionatos, O. 2006, *ApJL*, 643, L17
- Grillmair, C. J., & Dionatos, O. 2006, *ApJL*, 641, L37
- Helmi, A., & de Zeeuw, P. T. 2000, *MNRAS*, 319, 657
- Helmi, A., White, S. D. M., de Zeeuw, P. T., & Zhao, H. 1999, *Nature*, 402, 53
- Johnston, K. V., Zhao, H., Spergel, D. N., & Hernquist, L. 1999, *ApJL*, 512, L109
- Ibata, R. A., Gilmore, G., & Irwin, M. J. 1994, *Nature*, 370, 194
- Kafle, P. R., Sharma, S., Robotham, A. S. G., et al. 2017, *MNRAS*, 470, 2959
- Liu, C., Xu, Y., Wan, J.-C., et al. 2017, *Research in Astronomy and Astrophysics*, 17, 096
- Liu, C., Deng, L.-C., Carlin, J. L., et al. 2014, *ApJ*, 790, 110
- Mateu, C., Read, J. I., & Kawata, D. 2018, *MNRAS*, 474, 4112
- McMillan, P. J. 2017, *MNRAS*, 465, 76
- Morrison, H. L., Flynn, C., & Freeman, K. C. 1990, *AJ*, 100, 1191
- Reid, M. J., Menten, K. M., Brunthaler, A., et al. 2014, *ApJ*, 783, 130
- Rockosi, C. M., Odenkirchen, M., Grebel, E. K., et al. 2002, *AJ*, 124, 349
- Sanderson, R. E., Helmi, A., & Hogg, D. W. 2015, *ApJ*, 801, 98
- Schönrich, R., Binney, J., & Dehnen, W. 2010, *MNRAS*, 403, 1829
- Schönrich, R., & Aumer, M. 2017, *MNRAS*, 472, 3979
- Smith, M. C., Evans, N. W., Belokurov, V., et al. 2009, *MNRAS*, 399, 1223
- Tian, H.-J., Liu, C., Carlin, J. L., et al. 2015, *ApJ*, 809, 145
- Xu, Y., Liu, C., Xue, X.-X., et al. 2018, *MNRAS*, 473, 1244
- Zhao, G., Zhao, Y.-H., Chu, Y.-Q., Jing, Y.-P., & Deng, L.-C. 2012, *Research in Astronomy and Astrophysics*, 12, 723
- York, D. G., Adelman, J., Anderson, J. E., Jr., et al. 2000, *AJ*, 120, 1579